Monthly Notices
of the
ROYAL ASTRONOMICAL SOCIETY

MNRASL , L90–L94 (2014)
Advance Access publication 2014 January 30

doi:10.1093/mnrasl/slu004

The polluted atmospheres of cool white dwarfs and the magnetic field connection⋆

Adéla Kawka† and Stéphane Vennes†

Astronomický ústav, Akademie věd České republiky, Fričova 298, CZ-251 65 Ondřejov, Czech Republic

Accepted 2014 January 6. Received 2013 December 14; in original form 2013 October 19

ABSTRACT

We present an analysis of X-Shooter spectra of the polluted hydrogen-rich white dwarfs (DAZ) NLTT 888 and NLTT 53908. The spectra of NLTT 53908 show strong, Zeeman-split calcium lines (Ca II H&K and Ca I λ4226) and the star appears to be a close relative of the polluted magnetic white dwarf (DAZH) NLTT 10480, while the spectra of NLTT 888 show narrow lines of calcium and iron. A comparison of the DAZ NLTT 888 and the DAZH NLTT 53908 with other class members illustrates the diversity of environment and formation circumstances surrounding these objects. In particular, we find that the incidence of magnetism in old, polluted white dwarfs significantly exceeds that found in the general white dwarf population which suggests a hypothetical link between a crowded planetary system and magnetic field generation.

Key words: white dwarfs – stars: abundances – stars: atmospheres – stars: individuals: NLTT 888 – stars: individuals: NLTT 53908 – stars: magnetic field.

1 INTRODUCTION

Polluted white dwarfs provide an opportunity to investigate the ultimate fate of planetary systems. Villaver & Livio (2007) show that under the right conditions, some planets do manage to survive the asymptotic giant branch (AGB) and post-AGB phases, while Debes & Sigurdsson (2002) had already shown that these planets and asteroids could find themselves within the white dwarf tidal radius if their orbits become unstable during close encounters with each other. The formation of debris discs around white dwarfs may be a common occurrence (Jura 2003; Kilic et al. 2006) and is most likely related to the presence of a crowded circumstellar environment in the parent star. The presence of debris material accreted on to the white dwarf surface is evident in spectroscopic observations of a large fraction of hydrogen-rich white dwarfs (Zuckerman et al. 2003).

The origin of magnetic fields in white dwarf stars may be linked to possible field-generating merger events preceding the birth of the white dwarf (Tout et al. 2008; Nordhaus et al. 2011; García-Berro et al. 2012). The likelihood of such mergers during the post-AGB phase would be directly related to the multiplicity in their respective stellar or planetary systems: surface metallicity and magnetic field in white dwarfs may be concomitant.

Recent investigations have uncovered several cool, magnetic, polluted DA white dwarfs (Farihi et al. 2011; Kawka & Vennes 2011; Zuckerman et al. 2011). Because the initial class identifications were secured with low-dispersion spectra, the present DAZ selection is independent of field intensity weaker than ∼1 MG. The inverse problem remains to be investigated: Could some high-field white dwarfs also be polluted? An answer to that question would require detailed modelling beyond linear Zeeman effect, but spectral lines could still escape detection because of line spread.

We present an analysis of two recently identified polluted white dwarfs from the revised NLTT catalogue of Salim & Gould (2003): NLTT 888 and the magnetic white dwarf NLTT 53908. In Section 2, we present new high signal-to-noise ratio spectra of these objects. With these data, we constrain the atmospheric parameters (Section 3.1), the magnetic field strength in NLTT 53908 (Section 3.2) and we conduct an abundance analysis (Section 3.3). Finally, we summarize our results in Section 4 and examine the particular case of NLTT 53908 along with the class properties of cool, magnetic DAZ white dwarfs.

2 OBSERVATIONS

We first observed NLTT 53908 with the ESO Faint Object Spectrograph and Camera attached to the New Technology Telescope at La Silla Observatory on UT 2008 October 21. We used grism number 11 (300 lines/mm) with a 1 arcsec slit-width resulting in a resolution of $\Delta\lambda \sim 14$ Å. The spectrum revealed a cool DAZ white dwarf with Ca II H&K. Incidentally, Limoges, Lépine & Bergeron (2013) classified NLTT 53908 (PM I 22276+1753) as a DA white dwarf.

⋆Based on observations collected at the European Organisation for Astronomical Research in the Southern Hemisphere, Chile, under programmes ID 082.D-0750 and 091.D-0267.

† E-mail: kawka@sunstel.asu.cas.cz (AK); vennes@sunstel.asu.cas.cz (SV)

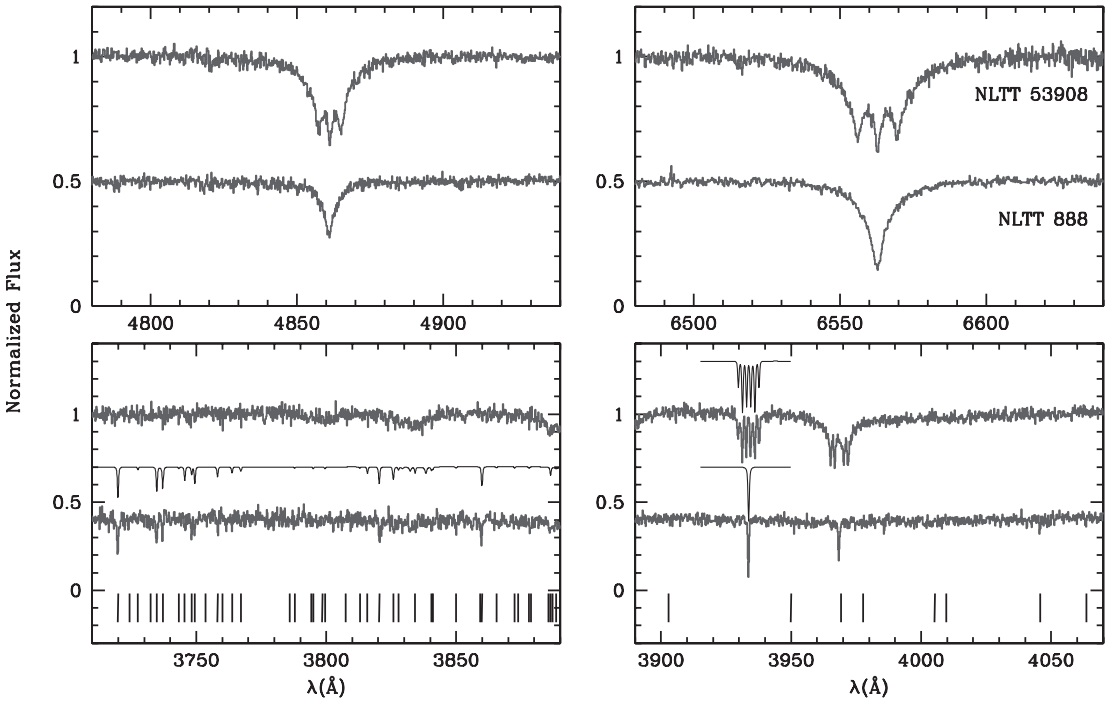

Figure 1. Sections of the X-shooter spectra (grey lines) of NLTT 888 (offset −0.5 in the top panels and −0.6 in the lower panels) and NLTT 53908 from 3710 to 6650 Å. All iron lines with a strength $\log gf > -1.2$ and a lower energy level $E_{\rm low} < 20\,000$ cm^{-1} are marked with vertical lines. Table 1 lists all prominent lines. The lower panels also show best-fitting models to calcium and iron lines (black lines) shifted by +0.3 relative to the observed spectra (see Section 3.3).

Following up on our own classification, we obtained two sets of echelle spectra of NLTT 53908 using the X-shooter spectrograph (Vernet et al. 2011) attached to the UT2 (Kueyen) at Paranal Observatory on UT 2013 July 10 and August 9. The spectra were obtained with the slit-width set to 0.5, 0.9 and 0.6 arcsec for the UVB, VIS and NIR arms, respectively. This setup delivered a resolution of $R = \lambda/\Delta\lambda = 9900$, 7450 and 7780 for the UVB, VIS and NIR arms, respectively. The exposure times were 2940 and 3000 s for the UVB and VIS arms, respectively. For the NIR arm, we obtained five exposures of 600 s each. The observations were conducted at the parallactic angle.

We first observed NLTT 888 with Focal Reducer and low dispersion Spectrograph (FORS2) attached to the UT2. Based on these spectropolarimetric data, Kawka & Vennes (2012b) placed an upper limit of 40 kG on the longitudinal magnetic field. The blue FORS2 spectrum revealed a cool DAZ white dwarf showing Ca II H&K absorption lines with an abundance of $\log {\rm Ca/H} = -10.65 \pm 0.15$ (Kawka & Vennes 2012b). Consequently, we obtained a set of six X-shooter spectra on UT 2013 August 4, September 2 and September 3. The observations were conducted with the configuration and exposure times described earlier. The spectra (Fig. 1) confirmed the Ca II line identifications and, in addition, revealed several Fe I lines. Table 1 lists all strong lines along with their respective equivalent widths and heliocentric velocities. The Hα core appears rounded or possibly split by the effect of an ∼30 kG field. The heavy element line velocities average 17.5 ± 5.2 km s^{-1} and are marginally consistent with the Hα velocity (23.4 ± 2.0 km s^{-1}).

Table 2 lists available photometric measurements from the *Galaxy Evolution Explorer* (*GALEX*) sky survey, the Sloan Digital Sky Survey (SDSS), the Two Micron All Sky Survey (2MASS) and the *Wide-field Infrared Survey Explorer* (*WISE*). We describe in Section 3.1, the continuum temperature measurements using the photometric data.

Table 1. Equivalent widths and line velocities of NLTT 888.

Ion/λ[a] (Å)	EW (mÅ)	v (km s^{-1})	Ion/λ[a] (Å)	EW (mÅ)	v (km s^{-1})
Fe I 3440.735[b]	144.0	18.7	Fe I 3820.425	83.0	26.3
Fe I 3581.195	133.0	9.6	Fe I 3859.911	75.0	13.9
Fe I 3719.935	134.0	19.7	Ca II 3933.66	196.0	18.0
Fe I 3734.864	90.0	16.6	Ca II 3968.47	140.0	19.7
Fe I 3737.131	73.0	19.2	Fe I 4045.813	43.0	13.9
Fe I 3748.262	58.0	19.8	Fe I 4063.594	30.0	7.8
Fe I 3749.485	51.0	14.8	H I 4861.323	–	7.8
Fe I 3758.233	51.0	26.9	H I 6562.797	–	24.2

[a]Laboratory wavelength from the National Institute of Standards and Technology (NIST) which is accessible from http://www.nist.gov/pml/data/asd.cfm.
[b]Blend of Fe I 3440.606 and 3440.989 Å.

3 ANALYSIS

In our analysis of the atmospheric properties of NLTT 888 and NLTT 53908, we used a grid of hydrogen-rich model atmospheres calculated in local thermodynamic equilibrium. These models are described in Kawka & Vennes (2006) and Kawka & Vennes (2012a). We calculated masses and cooling ages using the evolutionary mass–radius relations of Benvenuto & Althaus (1999).

3.1 Atmospheric parameters and spectral energy distributions (SED)

First, we determined the effective temperature and surface gravity of NLTT 888 and NLTT 53908 by fitting the observed Balmer lines with grids of synthetic spectra using χ^2 minimization techniques (Fig. 2). For NLTT 888, we included Hα to H8, but excluded Hϵ

Table 2. Photometry.

Survey/band[a]	λ eff.	Magnitude	
		NLTT 888	NLTT 53908
GALEX NUV	2315 Å	22.416 ± 0.264	19.459 ± 0.077
SDSS *u*	3551 Å	19.011 ± 0.028	17.522 ± 0.011
SDSS *g*	4686 Å	17.983 ± 0.006	16.897 ± 0.004
SDSS *r*	6166 Å	17.536 ± 0.006	16.659 ± 0.005
SDSS *i*	7481 Å	17.352 ± 0.006	16.590 ± 0.005
SDSS *z*	8931 Å	17.344 ± 0.017	16.612 ± 0.010
2MASS *J*	1.235 μm	16.478 ± 0.104	15.853 ± 0.076
2MASS *H*	1.662 μm	16.348 ± 0.206	15.567 ± 0.117
2MASS *K*	2.159 μm	17.058:	15.466 ± 0.189
*WISE W*1	3.353 μm	16.293 ± 0.091	15.088 ± 0.045
*WISE W*2	4.603 μm	16.032 ± 0.254	15.313 ± 0.121

[a]*GALEX* GR6/GR7 photometry obtained at galex.stsci.edu/GalexView/; SDSS Photometric Catalog, Release 10 (Ahn et al. 2013); 2MASS photometry (Skrutskie et al. 2006); (*WISE*) photometry (Cutri et al. 2012).

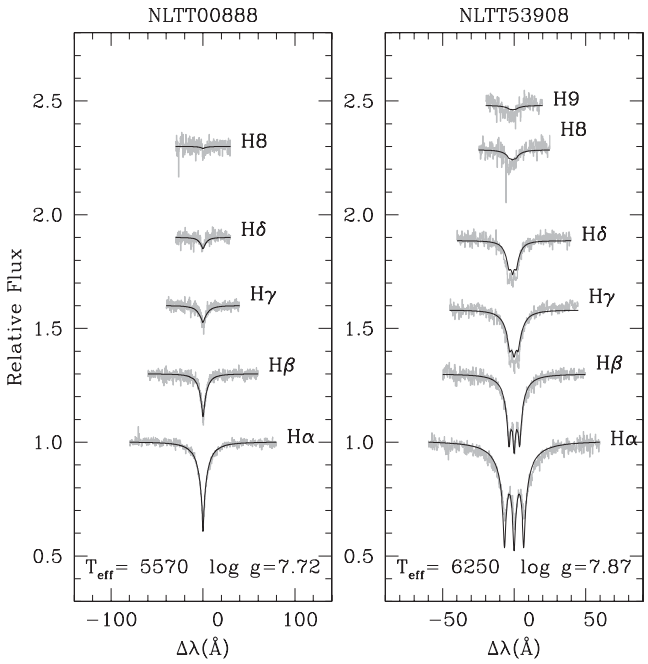

Figure 2. Balmer lines of NLTT 888 (left) and NLTT 53908 (right) compared to their corresponding best-fitting model spectra.

which is dominated by Ca II K. For NLTT 53908, we included Hα to H9, but again excluded Hϵ. For NLTT 53908, we also included the effect of a magnetic field on the line formation as described by Unno (1956) and Martin & Wickramasinghe (1981). However, the Hα core is poorly fitted: we neglected the effect of a field distribution associated with, for example, a dipolar field structure that would broaden the observed line profile. Instead, we assumed a single valued field.

Fig. 3 shows the observed and calculated SED for both objects. In the case of NLTT 888, the effective temperature determined from the Balmer line fits (5570 K) is consistent with the temperature determined from the SED (5590 K). However, for NLTT 53908, the effective temperature from the Balmer line fits (6250 K) is lower than the effective temperature required to match the observed SED (6465 K). Table 3 summarizes these measurements and lists additional properties derived from these measurements.

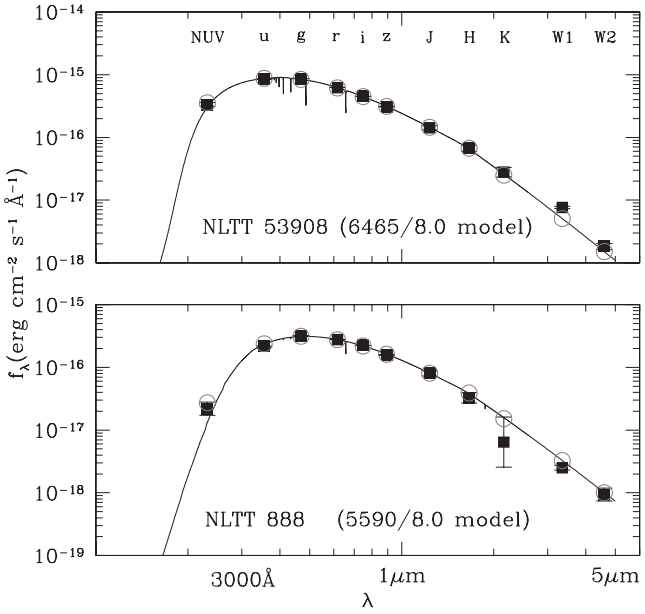

Figure 3. SED, f_λ (erg cm^{-2} s^{-1} Å^{-1}) versus λ, of NLTT 888 (bottom) and NLTT 53908 (top). The observed SED (full squares) was built using photometric data (Table 2), and the synthetic SED (open circles) was computed using best-fitting model (full line). We noted the possible detection of a mild infrared excess in NLTT 53908.

Table 3. Properties.

Parameter	NLTT 888	NLTT 53908
$T_{\rm eff}$ (K)	5570 ± 40	6250 ± 70
log *g* (cgs)	7.72 ± 0.08	7.87 ± 0.12
Mass ($M_\odot$)	0.45 ± 0.03	0.51 ± 0.07
Distance (pc)	58 ± 3	38 ± 3
Age (Gyr)	$4.0^{+1.8}_{-0.3}$	$1.7^{+0.5}_{-0.3}$
$T_{\rm eff}$ (K)[a]	5590 ± 50	6465 ± 55
log *g* (cgs)[a]	(8.0)	(8.0)
log Mg/H ([Mg/H][b])	<−8.7(−4.3)	<−7.9(−3.5)
log Si/H ([Si/H][b])	<−8.9(−4.4)	<−8.0(−3.5)
log Ca/H ([Ca/H][b])	−10.77(−5.10) ± 0.06	−9.85(−4.18) ± 0.04
log Fe/H ([Fe/H][b])	−9.01(−4.48) ± 0.07	<−8.7(−4.2)
$v_{\rm r}$ (km s^{-1})	23.4 ± 2.0	20.8 ± 1.5
$B_{\rm S}$ (kG)	<40	334 ± 3

[a]Based on the SED.
[b][X/H] = log *X*/H − log *X*/H$_\odot$.

3.2 Magnetic field

We measured the strength of the average surface magnetic field in NLTT 53908 using the Zeeman-split pattern of Hα and the calcium lines. Details of the predicted Zeeman line components are presented in Kawka & Vennes (2011). We fitted Gaussian functions to each Zeeman component of Ca I λ 4226 Å, Ca II H&K and Hα, and measured the line centres. Next, we simultaneously constrained the magnetic field strength and average line velocity by fitting the observed line centres with predicted positions. Using the calcium lines, we determined a surface averaged magnetic field of $B_{\rm S} = 0.335 \pm 0.003$ MG with a velocity of $v = 19.8 \pm 1.7$ km s^{-1}. Using Hα, we determined $B_{\rm S} = 0.331 \pm 0.004$ MG with a velocity of $v = 23.9 \pm 2.9$ km s^{-1}. The magnetic field measurements and velocities are consistent within uncertainties. We adopted the

weighted average of these measurements $B_S = 0.334 \pm 0.003$ MG and $v = 20.8 \pm 1.5\,\mathrm{km\,s^{-1}}$.

The Hα core in NLTT 888 shows the possible effect of broadening due to unresolved splitting by a weak field (∼30 kG). However, a higher resolution spectrum would be required to fully resolve the Zeeman pattern and confirm the magnetic field detection.

3.3 Abundance analysis

We initiated a study of the abundance patterns in NLTT 888 and 53908 by fitting a set of model spectra with varying abundances to the X-shooter spectra. For NLTT 888, we set the effective temperature and surface gravity to that determined from the Balmer line fits. However, for NLTT 53908, we adopted $T_{\rm eff} = 6300$ K ($\log g = 7.8$) as a compromise between the Balmer line fit and the SED analysis. For reference, we adopted the solar abundance scale described in Vennes & Kawka (2013) that was built using the compilations of Asplund et al. (2009) and Lodders, Palme & Gail-P. (2009). The measured abundances and upper limits are summarized in Table 3. The quoted uncertainties are statistical only (1σ), and we may add systematic errors of ∼0.1 dex due to model uncertainties (see below). The upper limits are taken at the 90 per cent confidence level.

The measured calcium ($\log \mathrm{Ca/H} = -10.77$) and iron ($\log \mathrm{Fe/H} = -9.01$) abundances imply that the atmosphere of NLTT 888 is iron enhanced ($\log \mathrm{Fe/Ca} = 1.76$). Note that if we assume $\log g = 8$, the abundances would be shifted up by 0.1 dex, while abundance ratios remain unaffected. The calcium abundance measured with X-shooter is in agreement with that originally determined by Kawka & Vennes (2012b) using FORS data ($\log \mathrm{Ca/H} = -10.65 \pm 0.15$). We calculated magnesium and silicon abundance upper limits, but were unable to secure meaningful constraints to the aluminium abundance.

Next, we measured the abundance of calcium in the atmosphere of NLTT 53908 and calculated upper limits for the abundance of magnesium, silicon and iron. We found a significant discrepancy in the abundance of calcium based on Ca I and Ca II lines. Using the Ca II H&K lines, we measured $\log \mathrm{Ca/H} = -9.85 \pm 0.04$ ($[\mathrm{Ca/H}] = -4.18 \pm 0.04$) compared to $\log \mathrm{Ca/H} = -9.24^{+0.10}_{-0.19}$ ($[\mathrm{Ca/H}] = -3.57^{+0.10}_{-0.19}$) using the Ca I λ4226 line. A similar problem was also encountered in our analysis of the cool magnetic DAZ NLTT 10480 (Kawka & Vennes 2011). In this case, adopting a cooler atmosphere helped restore the calcium ionization balance. However, in the case of NLTT 53908, a lower effective temperature that would restore consistency is excluded by the SED and Balmer line fits. A surface gravity shift of 0.3 dex results in abundance shift of 0.06 dex in both Ca I and Ca II measurements, leaving the ionization ratio virtually unchanged. Also, a change in temperature of −200 K results in abundance shifts of 0.25 and 0.15 using Ca I and Ca II lines, respectively, corresponding to a change in the Ca I/Ca II ionization ratio of 0.1 dex. Such small variations do not resolve the present difficulties with the calcium ionization balance. Because Ca II is the dominant ionization species we adopted the abundance measurement based on the Ca II lines. The calcium abundance and the upper limits offer a glimpse of the composition of NLTT 53908 and we may conclude that its atmosphere is not iron enhanced.

4 SUMMARY AND DISCUSSION

We obtained accurate calcium abundance measurements in the atmospheres of the DAZ white dwarfs NLTT 53908 and NLTT 888. Also, we measured the iron abundance in NLTT 888 and found that NLTT 53908 is a magnetic white dwarf. These two objects join a class of cool, polluted white dwarfs. Table 4 lists all DAZ white dwarfs with $T_{\rm eff} < 7000$ K. Their atmospheric parameters and abundance measurements are taken from the cited references. It is worth noting that within this sample of cool DAZ white dwarfs, the iron to calcium abundance ratio varies by a factor of ∼50 from an abundance ratio close to unity (NLTT 43806) and up to ∼60 (NLTT 888), and assuming steady-state accretion, this range of abundances suggests a remarkable diversity in the accretion source composition.

Also, Table 4 lists confirmed surface magnetic fields B_S or upper limits based on the shape of the Hα core. Requiring that the σ components occupy separate resolution elements, we have $\lambda R^{-1} = \Delta\lambda_B$, where R is the resolving power and λ_B is the magnetic line displacement. We find that $B \lesssim 235\, g/\lambda$ kG, where g is the Landé factor and λ is given in Å. For those stars that have been observed spectropolarimetrically, we provide the longitudinal magnetic field $|B_l|$ measurement or upper limit. Out of 13 objects listed in Table 4, 4 are known to possess a magnetic field. Restricting the sample to temperatures below 6000 K, seven objects remain with three harbouring a magnetic field.

The incidence of magnetism in the general population of white dwarfs has been reported to be as low as ∼5 per cent in spectropolarimetric surveys (Schmidt & Smith 1995; Kawka & Vennes

Table 4. Known cool DAZ white dwarfs ($T_{\rm eff} < 7000$ K).

WD	Name	$T_{\rm eff}$ (K)	$\log g$ (c.g.s)	log (Ca/H)	Fe/Ca	B_S (kG)	$\lvert B_l\rvert$ (kG)	Reference
WD0015−055	NLTT 00888	5570 ± 40	7.72 ± 0.08	−10.77 ± 0.06	58	<40	<40	1,2
WD0028+220	NLTT 01675	6020 ± 50	8.04 ± 0.07	−9.53 ± 0.03	8	<40	–	3
WD0151−308	NLTT 06390	6040 ± 40	7.90 ± 0.07	−10.00 ± 0.04	27	<40	<11	2,3
WD0243−026	LHS 1442	6800 ± 300	8.15 ± 0.10	−9.90	–	<10	–	4
WD0245+541	G 174-14	5190 ± 300	8.22 ± 0.10	−12.69	–	<10	–	4
WD0315−293	NLTT 10480	5200 ± 200	8.0 ± 0.5	−10.3 ± 0.3	<10	519 ± 4	212 ± 50	3,5
WD0322−019	G 77-50	5310 ± 100	8.05 ± 0.01	−9.8 ± 0.2	13	120	–	6
WD0334−224	NLTT 11393	5890 ± 30	7.86 ± 0.06	−10.24 ± 0.04	<7	<40	<16	2,3
WD1208+576	G 197-47	5830 ± 300	7.91 ± 0.10	−10.96	–	<10	–	4
WD1344+106	G 63-54	6945 ± 300	7.99 ± 0.10	−11.13	–	<10	–	4
WD1633+433	G 180-63	6570 ± 300	8.08 ± 0.10	−8.63	5	<10	–	4
WD1653+385	NLTT 43806	5900	8.0	−7.9 ± 0.19	1.3	70	–	7
WD2225+176	NLTT 53908	6250 ± 70	7.87 ± 0.12	−9.85 ± 0.04	<13	334 ± 3	–	1

References: (1) This work; (2) Kawka & Vennes (2012b); (3) Kawka & Vennes (2012a); (4) Zuckerman et al. (2003); (5) Kawka & Vennes (2011); (6) Farihi et al. (2011); (7) Zuckerman et al. (2011).

2012b) to possibly as high as 13–21 per cent in the old population of nearby white dwarfs (Kawka et al. 2007). The field strengths range from a few kG (see, e.g., Landstreet et al. 2012) to several 100 MG covering five orders of magnitude. Assuming a flat distribution per field decade (Schmidt & Smith 1995; Kawka et al. 2007), we estimate that 40 per cent of magnetic white dwarfs have fields below 1 MG (corresponding to the largest field in our DAZ sample), i.e. ∼7 per cent of the old, local population. Assuming that our DAZ sample was drawn from a similar population, we find that the probability of identifying 4 magnetic white dwarfs in a sample of 13 objects is below 1 per cent. Therefore, we can be confident at the 99 per cent level that the population of cool DAZ white dwarfs has a higher incidence of magnetism than currently reported in the general population. For example, Bergeron, Ruiz & Leggett (1997) reported the identification of 12 magnetic white dwarfs in a survey of ∼110 cool white dwarfs ($4000 \lesssim T_{\rm eff} \lesssim 10\,000$ K) or an incidence of 11 per cent. More specifically, 8 out of 64 hydrogen-rich white dwarfs (13 per cent) were found to be magnetic, with only 2 objects with a field below 1 MG. The probability that our sample of 4 magnetic objects out of 13 DAZ white dwarfs could be drawn from a population with a 3 per cent (2/64) field incidence is below 0.1 per cent. Important questions remain unanswered: first, having estimated the field incidence among cool, polluted white dwarfs, what would be the incidence among their warmer ($T_{\rm eff} \gtrsim 10\,000$ K) counterparts? Conversely, what would be the fraction of polluted white dwarfs in a high-field (>1 MG) sample? In the context of merger-induced magnetic fields (Tout et al. 2008; Nordhaus et al. 2011; García-Berro et al. 2012; Külebi et al. 2013; Wickramasinghe, Tout, & Ferrario 2014), only mergers occurring on the red giant or asymptotic red giant phases generate fields. Also, diffusion models (see, e.g., Koester 2009) imply that atmospheric pollution quickly recedes after an accretion event. A dense circumstellar environment increases the probability that these events would be observed simultaneously in a given system.

ACKNOWLEDGEMENTS

AK and SV are supported by the GAČR (P209/12/0217, 13-14581S) and the project RVO:67985815.

This publication makes use of data products from *WISE*, which is a joint project of the University of California, Los Angeles and the Jet Propulsion Laboratory/California Institute of Technology, funded by the National Aeronautics and Space Administration, and from 2MASS, which is a joint project of the University of Massachusetts, and the Infrared Processing and Analysis Center/California Institute of Technology, funded by the National Aeronautics and Space Administration and the National Science Foundation.

REFERENCES

Ahn C. P. et al., 2013, ApJS, preprint (arXiv:1307.7735)
Asplund M., Grevesse N., Sauval A. J., Scott P., 2009, ARA&A, 47, 481
Benvenuto O. G., Althaus L. G., 1999, MNRAS, 303, 30
Bergeron P., Ruiz M. T., Leggett S. K., 1997, ApJS, 108, 339
Cutri R. M. et al., 2012, VizieR Online Data Catalog, 2311, 0
Debes J. H., Sigurdsson S., 2002, ApJ, 572, 556
Farihi J., Dufour P., Napiwotzki R., Koester D., 2011, MNRAS, 413, 2559
García-Berro E. et al., 2012, ApJ, 749, 25
Jura M., 2003, ApJ, 584, L91
Kawka A., Vennes S., 2006, ApJ, 643, 402
Kawka A., Vennes S., 2011, A&A, 532, A7
Kawka A., Vennes S., 2012a, MNRAS, 425, 1394
Kawka A., Vennes S., 2012b, A&A, 538, A13
Kawka A., Vennes S., Schmidt G. D., Wickramasinghe D. T., Koch R., 2007, ApJ, 654, 499
Kilic M., von Hippel T., Leggett S. K., Winget D. E., 2006, ApJ, 646, 474
Koester D., 2009, A&A, 498, 517
Külebi B., Ekşi K. Y., Lorén-Aguilar P., Isern J., García-Berro E., 2013, MNRAS, 431, 2778
Landstreet J. D., Bagnulo S., Valyavin G. G., Fossati L., Jordan S., Monin D., Wade G. A., 2012, A&A, 545, A30
Limoges M.-M., Lépine S., Bergeron P., 2013, AJ, 145, 136
Lodders K., Palme H., Gail H.-P., 2009, Landolt-Börnstein, New Ser., VI/4B, 560
Martin B., Wickramasinghe D. T., 1981, MNRAS, 196, 23
Nordhaus J., Wellons S., Spiegel D. S., Metzger B. D., Blackman E. G., 2011, Proc. Natl. Acad. Sci., 108, 3135
Salim S., Gould A., 2003, ApJ, 582, 1011
Schmidt G. D., Smith P. S., 1995, ApJ, 448, 305
Skrutskie M. F. et al., 2006, AJ, 131, 1163
Tout C. A., Wickramasinghe D. T., Liebert J., Ferrario L., Pringle J. E., 2008, MNRAS, 387, 897
Unno W., 1956, PASJ, 8, 108
Vennes S., Kawka A., 2013, ApJ, 779, 70
Vernet J. et al., 2011, A&A, 536, A105
Villaver E., Livio M., 2007, ApJ, 661, 1192
Wickramasinghe D. T., Tout C. A., Ferrario L., 2014, MNRAS, 437, 675
Zuckerman B., Koester D., Reid I. N., Hünsch M., 2003, ApJ, 596, 477
Zuckerman B., Koester D., Dufour P., Melis C., Klein B., Jura M., 2011, ApJ, 739, 101

This paper has been typeset from a TEX/LATEX file prepared by the author.